Earthquakes and Structures, *Vol. 8, No. 5 (2015) 1017-1038*
DOI: http://dx.doi.org/10.12989/eas.2015.8.5.1017

Strengthening of non-seismically designed beam-column joints by ferrocement jackets with chamfers

Bo Li[1], Eddie Siu-shu Lam[*1], Yuk-kit Cheng[1], Bo Wu[2] and Ya-yong Wang[3]

[1]*Department of Civil & Environmental Engineering, The Hong Kong Polytechnic University, Hong Kong, China*
[2]*School of Civil Engineering & Transportation, South China University of Technology, Guangzhou, China*
[3]*Institute of Earthquake Engineering, China Academy of Building Research, Beijing, China*

(Received April 11, 2014, Revised July 30, 2014, Accepted August 15, 2014)

Abstract. This paper presents a strengthening method that involves the use of ferrocement jackets and chamfers to relocate plastic hinge for non-seismically designed reinforced concrete exterior beam-column joints. An experimental study was conducted to assess the effectiveness of the proposed strengthening method. Four half-scale beam-column joints, including one control specimen and three strengthened specimens, were prepared and tested under quasi-static cyclic loading. Strengthening schemes include ferrocement jackets with or without skeleton reinforcements and one or two chamfers. Experimental results have indicated that the proposed strengthening method is effective to move plastic hinge from the joint to the beam and enhance seismic performance of beam-column joints. Shear stress and distortion within the joint region are also reduced significantly in strengthened specimens. Skeleton reinforcements in ferrocement provide limited improvement, except on crack control. Specimen strengthened by ferrocement jackets with one chamfer exhibits slight decrease in peak strength and energy dissipation but with increase in ductility as compared with that of two chamfers. Finally, a method for estimating moment capacity at beam-column interface for strengthened specimen is developed. The proposed method gives reasonable prediction and can ensure formation of plastic hinge at predetermined location in the beam.

Keywords: strengthening; beam-column joints; plastic hinge relocation; seismic performance; ferrocement jackets

1. Introduction

In the regions with low to moderate seismic risk, such as Hong Kong, there is no seismic consideration on design and detailing of reinforced concrete (RC) buildings (Lam *et al*. 2002). Thus, beam-column joints with no transverse reinforcement are not uncommon in existing RC buildings. In a moment resisting structure, beam-column joints are critical members to transfer forces between the beams and the columns and to maintain stability of structure (Paulay and Priestley 1992). Failure of beam-column joints due to the absent of seismic detailing has been widely observed in post-earthquake investigations (Sezen *et al*. 2003, Kam *et al*. 2011). In order to

*Corresponding author, Associate Professor, E-mail: cesslam@polyu.edu.hk

 ISSN: 2092-7614 (Print), 2092-7622 (Online)

minimize possible damage caused by earthquakes, an effective and economical strengthening technique is needed for improving the seismic performance of non-seismically designed beam-column joints.

Many strengthening and rehabilitation techniques have been proposed to upgrade non-seismically designed RC beam-column joints, including concrete jacketing (Alcocer and Jirsa 1993, Hakuto *et al.* 2000, Karayannis *et al.* 2008), steel jacketing (Ghobarah *et al.* 1997), epoxy injection (Karayannis *et al.* 1998), fiber reinforced polymer (FRP) wrapping (Ghobarah and Said 2002, Antonopoulos and Triantafillou 2003, Prota *et al.* 2004, Pantelides *et al.* 2008, Li and Chua 2009, Alsayed *et al.* 2010, Ilki *et al.* 2011, Li and Qian 2011, Sezen 2012), etc. Combined use of the above-mentioned methods has also been proposed for strengthening beam-column joints (Karayannis and Sirkelis 2008, Sasmal *et al.* 2011). Each strengthening method has particular advantages and limitations. Concrete jacketing is labor-intensive and increases member size. Additional protection is needed for steel jacketing to prevent potential corrosion and for fire protection. FRP wrapping eliminates most of the above-mentioned limitations, but fire insulation is required. Detailed review on strengthening techniques for beam-column joints can be referred to Engindeniz *et al.* (2005) and Bousselham (2010). Generally, the above-mentioned techniques enhance shear resistance of beam-column joints through external strengthening.

Strengthening of beam-column joints can also be achieved by reducing shear force input to the joint. Due to moment reversal across the joint, larger shear force will be formed in the joint as compared with adjoining members. Pampanin *et al.* (2006) developed a metallic haunch seismic retrofit system to reduce internal force for under-designed beam-column joints. Diagonal haunches installed at beam-column corners significantly reduced moments and shear forces in the joints. Two types of connection between haunch and joint, namely hinged and welded, were examined. Ends of haunches were fixed to the beams and columns using pre-stressed external rods. Alternatively, Genesio *et al.* (2011) used fully fastened end plate to connect haunch and joint. Generally, strengthening of beam-column joints using haunch with proper protection against corrosion and fire can significantly reduce the internal forces in joint region.

It is generally recognized that yielding at beam-column interface has detrimental effect on beam-column joints. Strength and stiffness degradation in a joint would occur due to strain penetration of beam reinforcements. Thus, code recommendation requires a high percentage of transverse reinforcement to avoid or minimize joint damage (Abdel-Fattah and Wight 1987). Beam-column joints designed without seismic detailing may suffer severe damage under cyclic loading. Relocation of plastic hinge away from the column face through enlarging joint area could enhance shear resistance and improve bonding conditions of beam reinforcement. Initially, this method was developed for new construction by detailing of reinforcements around the joint region. Abdel-Fattah and Wight (1987) relocated plastic hinge away from column face by supplementing intermediate longitudinal reinforcement over a specific length of the beam adjacent to the joint. Yi *et al.* (1996) achieved relocation of plastic hinge through using vertically anchored intermediate longitudinal reinforcement for exterior joints. Chutarat and Aboutaha (2003) proposed to relocate potential plastic hinge away from the column face by the use of headed reinforcements. For strengthening, Mahini and Ronagh (2011) retrofitted exterior beam-column joints using web-bonded FRP for plastic hinge relocation. These methods successfully delayed strength degradation and enhanced energy dissipation of beam-column joints. However, relocating plastic hinge increases the shear force applied to the joints.

In this paper, a combined method is proposed to strengthen non-seismically designed beam-column joints. Chamfers with ferrocement jackets are installed at beam-column corners to relocate

plastic hinge away from the joint as well as to reduce shear force transferred to the joint. Chaimahawan and Pimanmas (2009) applied four reinforced concrete chamfers at beam-column corners of interior joints to strengthen non-seismically designed beam-column joints. At the edges of chamfers, dowel bars were inserted to resist/transfer the shear forces and tensile forces. In this study, ferrocement jackets with chamfers are adopted to overcome the difficulties in embedding dowel bars into the joint. Ferrocement is a type of reinforced mortar with closely spaced layers of continuous and relatively small size wire mesh (ACI 549R 1997, Naaman 2000). Homogeneous and bidirectional properties of ferrocement may enhance the integrity of chamfers with the joint and may improve shear resistance of the joint (Li *et al.* 2013).

This study has also extended the existing research to embrace the use of one chamfer wrapped with ferrocement jacket to strengthen an exterior beam-column joint. This facilitates installation of a chamfer under the soffit of a beam with less implication on space. Even if a chamfer is to be installed on a floor slab (e.g., two chamfers), it can be readily hidden by an infill wall or partition.

To verify the above, four half-scale exterior beam-column joints, including one control specimen and three strengthened specimens, were tested to failure under reversed cyclic loading. Testing parameters include one chamfer or two chamfers as well as ferrocement jackets with or without skeleton reinforcements. Seismic performance of the tested specimens is examined in terms of hysteretic behavior, energy dissipation, stiffness degradation, ductility and joint behavior. Further, a simple method for estimating moment capacity at beam-column interface is developed for ferrocement-strengthened beam-column joints.

2. Experimental program

2.1 Specimens

The specimens are in half-scale and are identified as control specimen JC0 and strengthened

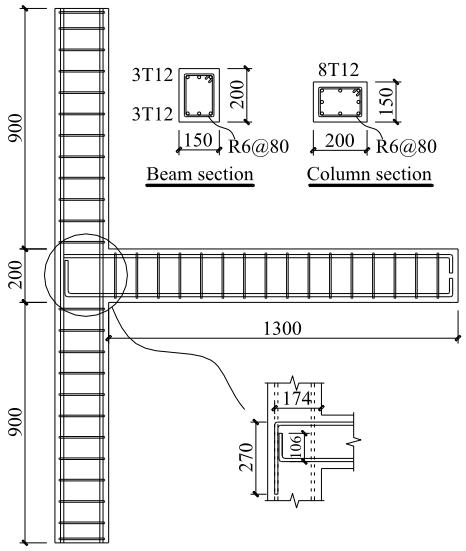

Fig. 1 Dimensions and reinforcement details of specimen

specimens JS1, JS2 and JS3. Reinforcement details of the specimens are identical representing typical exterior beam-column joints in moment resisting structures designed without seismic provision. Beams and columns have the same cross section of 150 mm width and 200 mm depth, and are 1300 mm and 2000 mm long respectively. Concrete cover is 15 mm to transverse reinforcements. Columns are reinforced with eight T12 high strength deformed bars. Main reinforcements of the beams are three T12 high strength deformed bars in both tension and compression zones. Full anchorage is provided to the top reinforcements whereas length of bend-up end is not less than 8ϕ for the bottom reinforcements (CopConcrete 1987). Here, ϕ is the bar diameter. Transverse reinforcements used in both beams and columns are R6 mild steel bars at 80 mm spacing. There is no transverse reinforcement in the joints. Dimensions and reinforcement details of the specimens are shown in Fig. 1.

2.2 Strengthening schemes

Specimens JS1, JS2 and JS3 were strengthened by ferrocement jackets with chamfers as illustrated in Fig. 2. Chamfers are proposed to be installed at beam-column corners while ferrocement jackets wrap the joint region and the chamfers. Strengthening schemes include ferrocement jackets with or without skeleton reinforcements and with one or two chamfers. The above aims to (1) move plastic hinge away from the joint; (2) reduce shear stress within the joint; and (3) protect the joint from severe damage.

Specimens JS1 and JS2 have two chamfers while specimen JS3 has one chamfer. Before wrapping ferrocement jackets, concrete cover in the joint region is first removed and surface of strengthening area is polished to enhance bonding between ferrocement jackets and concrete substrate. Dimension of the chamfers is 200 mm×200 mm including the ferrocement. The chamfers are integrated with the joints by ferrocement jackets. Specially, skeleton reinforcements using R6 mild steel bars are provided in the ferrocement for specimen JS1 only. Detail of the skeleton reinforcements is shown in Fig. 3(a). Anchorage of skeleton reinforcements is enhanced through welding the ends together. Potential plastic hinges in beams are expected to form at a distance from the joints. This prevents strength deterioration and stiffness degradation in the joints

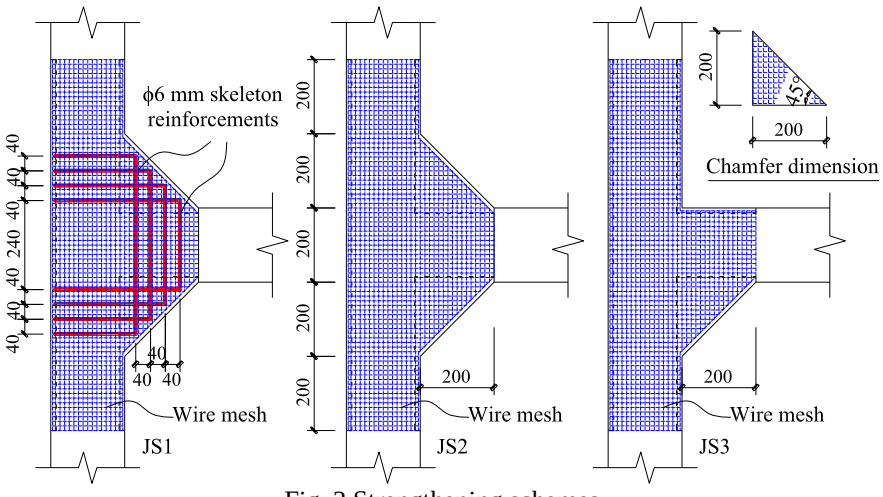

Fig. 2 Strengthening schemes

due to strain penetration from the plastic hinges. Potential plastic hinges are setback by a distance equal to the beam depth, i.e., 200 mm. Ferrocement jackets are also extended by 200 mm into the columns (with consideration of strong column weak beam behavior). One layer of wire mesh properly cut and folded is used to wrap around the joint as shown in Fig. 3(b) and Fig. 3(c). Finally, all specimens are grouted with high performance mortar. The chamfer is filled with the mortar used for ferrocement jacket.

2.3 Materials

All specimens were casted with the same ready-mixed concrete with maximum 10 mm aggregate. Before air curing, all specimens (including cubes and cylinders) were stored under moist condition. Mortar for ferrocement was prepared from a pre-mixed, non-shrinkage, high-performance cement-based mortar. Table 1 shows the material properties of concrete and mortar. Strengths of materials were estimated on the day of testing from three 100 mm cubes. Young's Moduli were determined 28 days after casting. Table 2 gives the mean strengths of reinforcements and wire mesh. High strength deformed bars were used as longitudinal reinforcements. Mild steel bars were adopted as transverse reinforcements and skeleton reinforcements. Square welded wire mesh was used in ferrocement. It has a diameter of 1.1 mm and a center-to-center spacing of 12.5 mm in both directions.

(a) (b) (c)

Fig. 3 Strengthening details of (a) skeleton reinforcements; (b) two chamfers; and (c) one chamfer

Table 1 Measured material properties of concrete and mortar for each specimen

Material		JC0	JS1	JS2	JS3
Concrete	Cube strength f_{cu} (MPa)	65.9	65.2	65.5	64.4
	Young's Modulus (GPa)		27.2		
Mortar	Cube strength f_{cu} (MPa)	--	73.5	81.7	68.0
	Young's Modulus (GPa)	--		27.8	

Table 2 Material properties of reinforcement and wire mesh

	Yield strength (MPa)	Ultimate strength (MPa)
T12	525.6	610.3
R6	350.0	420.0
Wire mesh	--	537.0 (Longitudinal) 508.0 (Transverse)

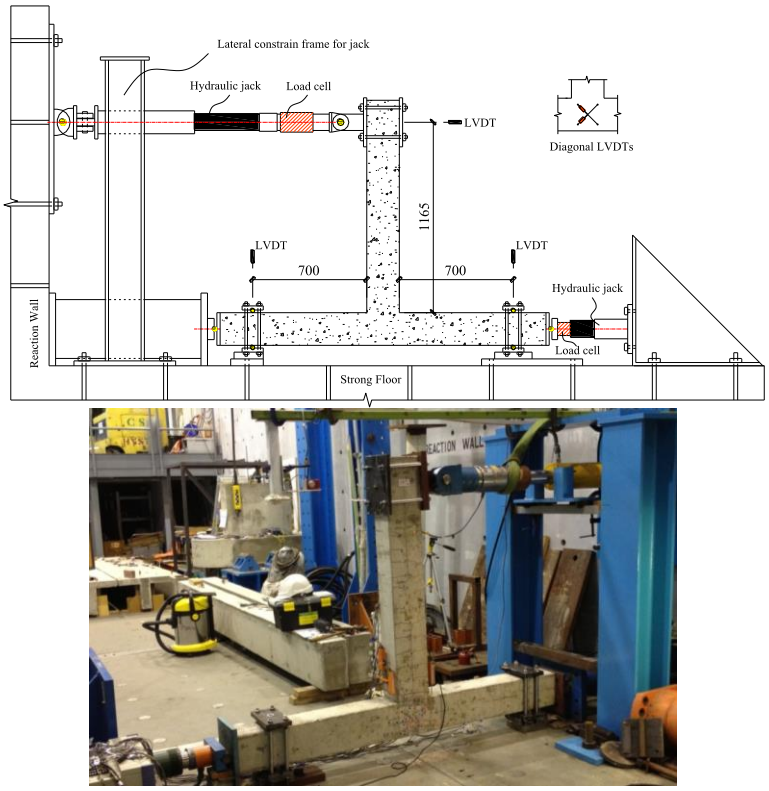

Fig. 4 Test setup

2.4 Test setup and instrumentations

Fig. 4 shows the test setup for exterior beam-column joints. A steel frame is installed to prevent out-of-plane movement. Ends of columns are restrained from translational movements and free to rotate. They are fixed to the strong floor and two LVDTs are installed to monitor the movement. Beam tip is connected to a hydraulic actuator through a hinge. The other end of the actuator is hinged to a reaction wall. Axial load is applied to column through a hydraulic jack. Reversed horizontal load is applied to the beam tip through a two-way hydraulic jack and is monitored by a load cell. Horizontal displacement at the beam tip is measured by a LVDT with 500 mm measurement range. A pair of LVDTs was installed diagonally in the joint to measure shear deformation. 16 strain gauges were installed on beam reinforcements and column reinforcements at critical locations.

2.5 Loading sequence

Axial load is first applied to column and is kept constant throughout the test. Magnitude of the axial load is $0.3f_c^{'}A_g$ which is common for structures without seismic consideration (Su *et al*. 2007, Li and Qian 2011). $f_c^{'}$ is the cylinder concrete strength and is assumed to be $0.8f_{cu}$. f_{cu} is the cube strength of concrete. A_g is the gross cross-sectional area of column. Subsequently, reversed cyclic loading is applied to the beam tip by a two-way actuator.

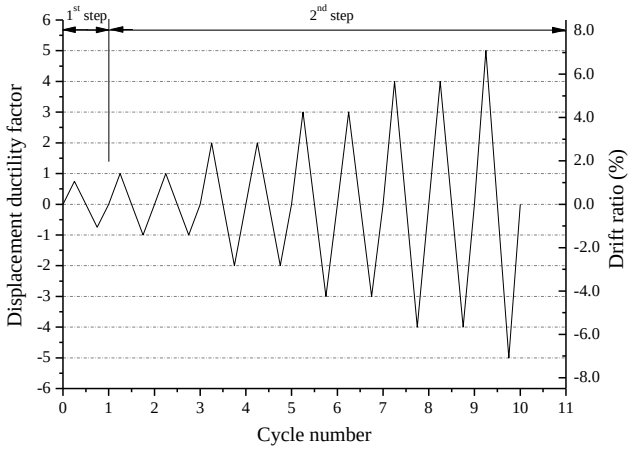

Fig. 5 Loading sequence

As shown in Fig. 5, horizontal loading is applied in two consecutive steps. The first step determines the yield displacement Δ_y (Park 1989). The specimen is subjected to a lateral force at 75% of ultimate moment capacity of the beam. With corresponding displacement at $\Delta_{0.75}$, yield displacement is $\Delta_y=\Delta_{0.75}/0.75$ based on linear extrapolation. In the second step, the beam tip is deflected with displacement ductility increasing from 1, 2, 3, etc. Displacement increment at each ductility factor is repeated twice. Corresponding drift ratio defined as displacement at beam tip divided by the length of beam is also illustrated in Fig. 5.

3. Experimental results and discussions

3.1 General behavior and failure modes

Fig. 6(a) shows the crack pattern of control specimen JC0. Flexural cracks were first observed at a drift ratio of 1.1% in the beam and before yielding of beam reinforcements. Subsequently, several cracks were formed in the joint at a drift ratio of 1.4%. With increase in drift ratio, cracks were primary formed at the beam-column interface and beam reinforcements yielded. Subsequently, cracks propagated into the joint and flexural cracks in the beam ceased to develop. Under cyclic loading, opening and closing of diagonal cracks in the joint resulted in concrete spalling at a drift ratio of 4.3%. Beam-column joints without transverse reinforcement failed in joint shear as shown in Fig. 7(a). With further increase in drift ratio, diagonal cracks in the joint were fully developed leading to severe damage in the joint. As a result, the columns could not sustain the applied axial load due to reduction of sectional area induced by spalling of concrete in the joint and column reinforcements buckled as shown in Fig. 7(b). It highlighted that axial failure of the column might be triggered by joint shear failure. It was worth noting that no flexural crack was observed in the column throughout the test. This may be attributed to applied axial load which reduced tensile strain along the column. Presence of shear failure mode confirms the weakness of the joint without seismic detailing.

Crack pattern of specimens JS1 is shown in Fig. 6(b). Flexural cracks in the beam and cracks at corners of the chamfers were first observed at a drift ratio of 1.1%. Following the development of

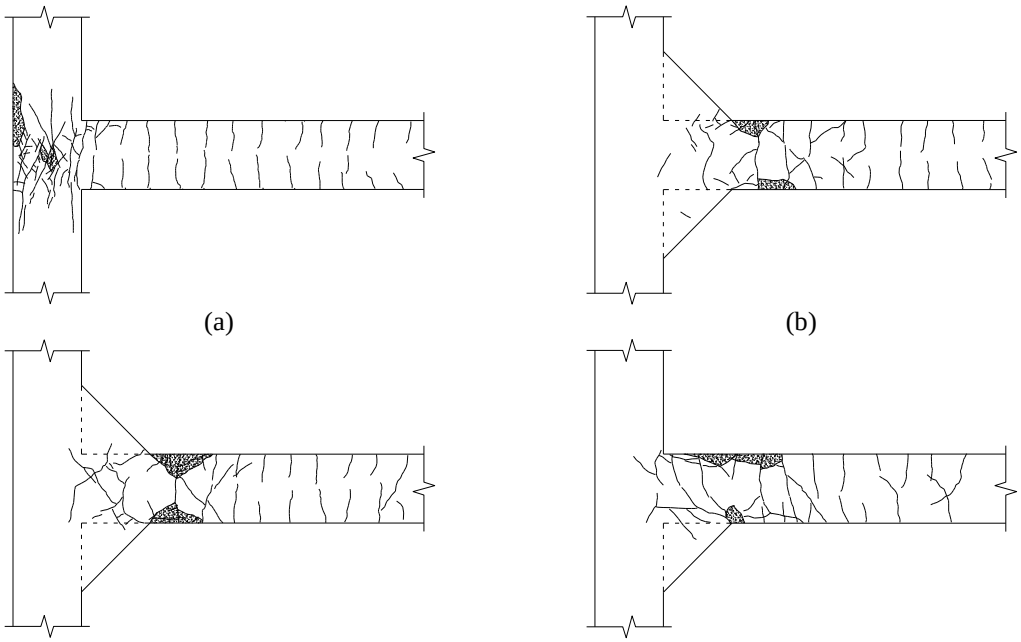

Fig. 6 Crack patters of specimens: (a) JC0, (b) JS1, (c) JS2 and (d) JS3

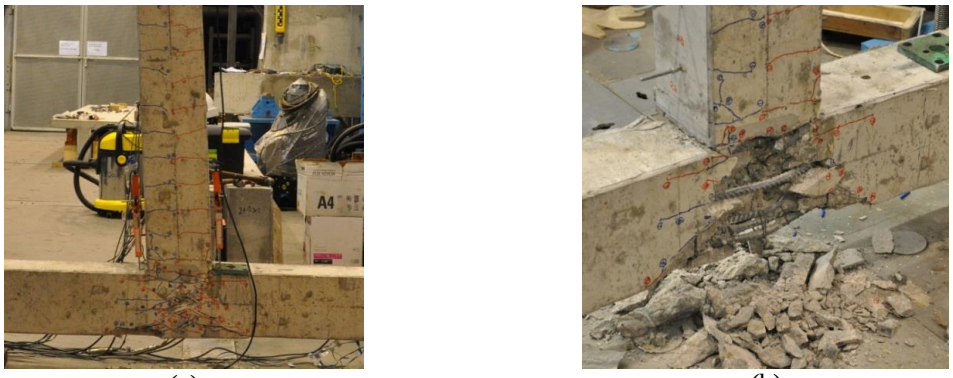

Fig. 7 Failure mode of specimen JC0: (a) diagonal cracking of joint core and (b) buckling of column reinforcements

interfacial cracks between un-strengthened area and strengthened area in the beam, several cracks were formed in the chamfers close to the beam at a drift ratio of 1.4%. After a drift ratio of 2.8%, no new crack was observed in the strengthened area and cracks were concentrated on plastic hinge zone next to the chamfers. Hence, shear capacity of the joint is properly ensured. In the advanced loading stage, fully developed cracks were observed in the beam's plastic hinge zone with spalling of concrete. No flexural crack was found in the column throughout the test. Finally, no new crack was found in the joint while a few new cracks developed in the chamfers. Specimen JS1 failed in beam-flexural mode as shown in Fig. 8(a). The proposed strengthening method is effective for relocating plastic hinge away from the joint and preventing failure of joint.

(a) (b) (c)

Fig. 8 Failure modes of strengthened specimens: (a) JS1, (b) JS2 and (c) JS3

Crack pattern of specimen JS2 are illustrated in Fig. 6(c). Before yielding of beam reinforcements, cracks were formed in the beam and the chamfers. With increase in drift ratio, cracks propagated gradually in the beam and in the chamfers. More cracks were observed in strengthening area of the beam as compared with that in specimen JS1. These cracks were extended into the joint. It illustrates that skeleton reinforcements in the chamfer provides better ability of crack control. Similar to specimen JS1, cracks in the chamfers ceased to propagate while more cracks were formed in plastic hinge zone close to the strengthened area after a drift ratio of 2.8%. No flexural crack was observed in the column. Finally, severe damage in the plastic hinge zone was observed in the beam due to repeated opening and closing of the cracks as shown in Fig. 8(b). Again, applying ferrocement jacket with two chamfers without skeleton reinforcements has changed the failure mode from joint-shear to beam-flexural. As compared with specimen JS1, more cracks were formed in the chamfers and extended to the joint due to the absence of skeleton reinforcements.

Crack pattern of specimen JS3 is shown in Fig. 6(d). Cracks were first formed in the beam and the chamfer. They were first extended to beam-column interface on the side without chamfer. Before reaching a drift ratio of 1.4%, flexural cracks were observed in the beam only. At a drift ratio of 2.8%, interfacial cracks were observed between the strengthened area and un-strengthened area of the beam. With the increase in drift ratio, spalling of concrete and mortar occurred at a drift ratio of 4.2%. As shown in Fig. 8(c), damage in the plastic hinge was more severe along the side without chamfer. Further, plastic hinge zone is closer to the joint as compared with that in specimens JS1 and JS2. However, the joint performed well with limited number of cracks extended into the joint. Finally, specimen JS3 failed at interface of strengthened area and un-strengthened area of the beam. Thus, a joint strengthened by ferrocement jacket with one chamfer also exhibits a ductile beam-flexural failure.

3.2 Hysteretic behavior

Plots of applied load versus displacement at beam tips for all specimens are given in Fig. 9. Lateral loads corresponding to flexural capacities of beam section at different locations are calculated and marked in Fig. 9. Flexural capacity of beam section is determined based on yielding of beam reinforcements. Generally, pinching effect is more obvious in the control specimen as

compared with the strengthened specimens. This is resulted from joint shear failure in control specimen. All specimens reach flexural capacities of beam section at failure. As a result, a plateau stage in load-displacement relationship is obtained for each specimen when approaching the peak load. However, yielding at beam-column interface in control specimen initiated joint shear failure with the effect of strain penetration. Sudden decrease in lateral load is observed after 4.3% drift for

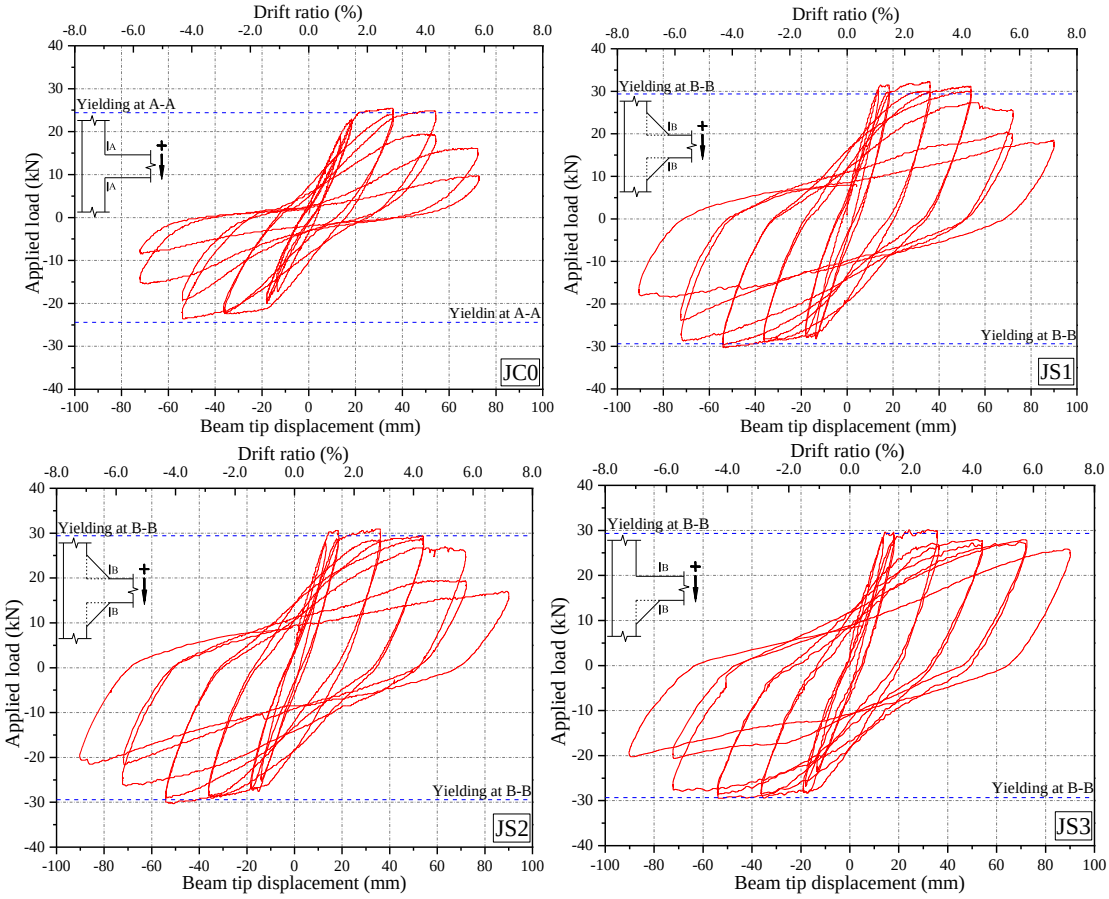

Fig. 9 Applied load versus displacement at beam tip for all specimens

Table 3 Summary of test results for all specimens

Specimen	Peak strength (kN)			Enhancement	Joint shear stress (MPa)	Failure modes
	Push	Pull	Mean			
JC0	25.5	-23.6	24.6	1.0	$0.68\sqrt{f_c'}$	Joint shear
JS1	32.4	-30.3	31.4	1.28	$0.35\sqrt{f_c'}$	Beam flexural
JS2	30.9	-30.3	30.6	1.25	$0.34\sqrt{f_c'}$	Beam flexural
JS3	30.2	-29.5	29.8	1.22	$0.34\sqrt{f_c'}$	Beam flexural

control specimen. In contrast, lateral loading capacities in strengthened specimens decrease gradually. Generally, all specimens are able to sustain the peak lateral loads at around drift ratio of 4.0%.

Envelops of hysteretic loops for all specimens are shown in Fig. 10 and summary of test results is given in Table 3. Loading capacities of the strengthened specimens are significantly improved as compared with that of the control specimen. Increase in peak lateral load for specimens JS1, JS2 and JS3 are 28%, 25% and 22% respectively. Peak strengths of the strengthened specimens are at similar level since failure was dominated by a beam-flexural mode. Improvement in peak strength is directly related to the relocation of plastic hinge from the joint to the beam next to strengthening area. It is essential to ensure that the chamfers have adequate strength. In this circumstance, ferrocement jackets reinforce the beam-joint and column-joint interfaces and confine the joints and the chamfers.

Specimen JS1 (with skeleton reinforcements in ferrocement) exhibits slightly higher peak strength as compared with specimen JS2. Specimen JS3 with one-side chamfer has relatively lower peak strength. This is possibly attributed to the movement of plastic hinge zone close to the joint leading to an increase in lever arm of the applied load. Nevertheless, one chamfer is preferred as it eliminates the obstruction caused by having a chamfer at the floor level.

3.3 Energy dissipation

Energy dissipation is calculated from the areas of hysteretic loops. Cumulative energy dissipation by the control specimen and strengthened specimens are shown in Fig. 11. Energy dissipated by strengthened specimens is significantly higher than that of the control specimen. This is mainly contributed to the failure of strengthened specimens in a ductile manner. Thus, all strengthened specimens exhibit similar energy dissipation capacity. Use of skeleton reinforcements in ferrocement jackets only slightly enhances the energy dissipation. Energy dissipated by specimen JS3 with one chamfer is less than the other strengthened specimens. In general, the

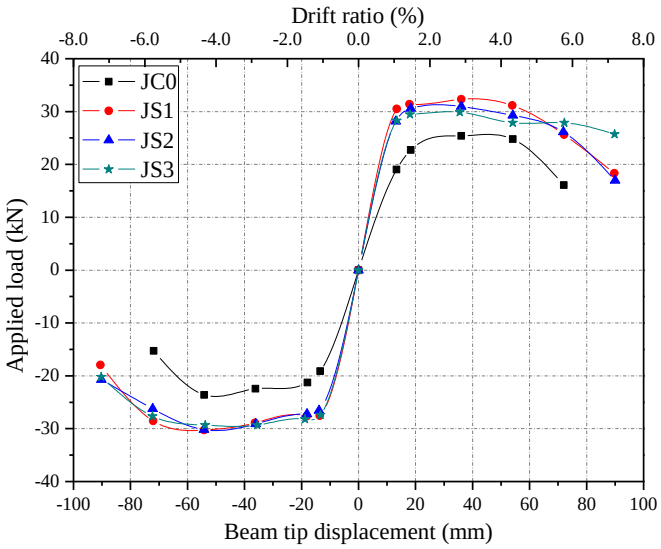

Fig. 10 Envelopes of hysteretic loops

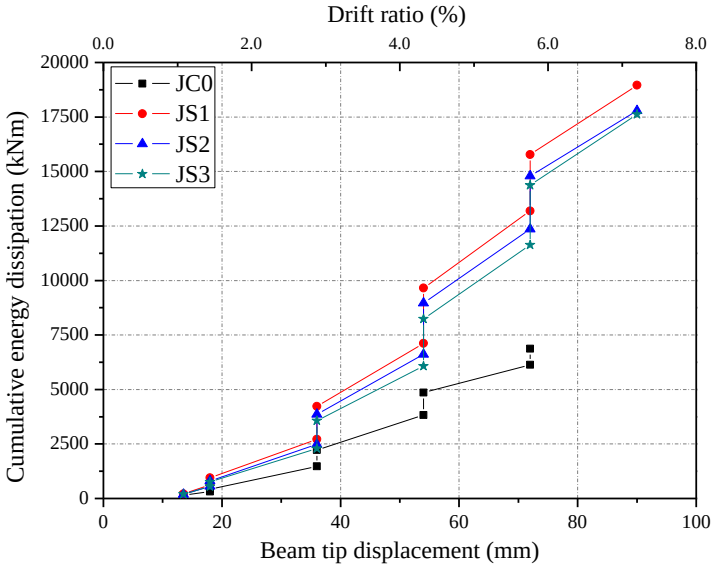

Fig. 11 Comparison of cumulative energy dissipation

proposed strengthening method is effective for enhancing energy dissipation capacity of exterior beam-column joints without seismic detailing. Influence of various strengthening schemes on energy dissipation is limited.

3.4 Stiffness degradation

Stiffness of a beam-column joint is estimated from the slope of a line passing through the positive maximum applied load and the negative maximum applied load in each hysteresis loop. Fig. 12 plots stiffness against beam tip displacement for each specimen. After strengthening, specimens JS1, JS2 and JS3 exhibit higher stiffness as compared with the control specimen at each drift ratio. Improvement in stiffness is directly contributed to relocation of plastic hinge away from the column face. Comparatively, higher stiffness is attained for specimen JS1 at the initial stage of loading. This may be attributed to the use of skeleton reinforcements in ferrocement. With the development of plastic hinges in the beams of strengthened specimens, their stiffness becomes similar at high drift ratio. Comparing specimens JS2 and JS3, number of chamfer has limited effect on stiffness. Generally, enhancement in stiffness is attributed to relocation plastic hinge which is achieved by strengthening.

3.5 Displacement ductility

Displacement ductility factor μ is defined as the ratio of ultimate displacement Δ_u to yield displacement Δ_y. Ultimate displacement is defined as the displacement corresponding to 15% drop of loading capacity. Yielding is estimated by balance of energy and general yielding (Li *et al.* 2013). Due to the relocation of plastic hinge, yield displacement is reduced. Improvement in ductility is normally reflected by an increase in ultimate displacement rather than decrease in yield displacement. Here, yield displacement for strengthened specimen is assumed to be that obtained

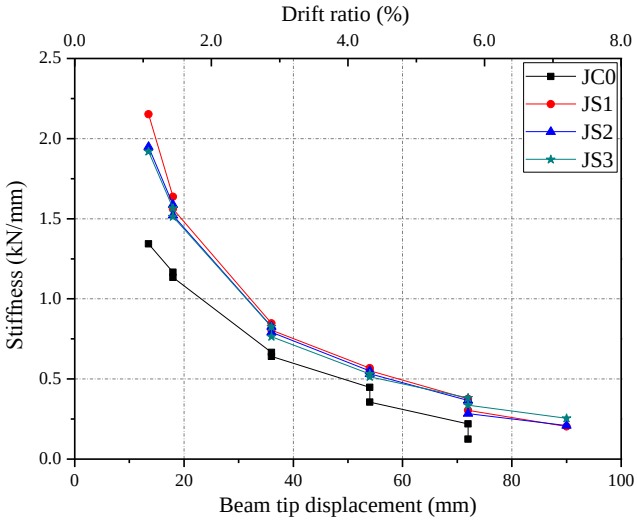

Fig. 12 Comparison of stiffness degradation

Table 4 Displacement ductility of control and strengthened specimens

Specimen	Δ_u (mm)	Balance of energy		General yield		Averaged μ
		Δ_y (mm)	μ	Δ_y (mm)	μ	
JC0	61.20	20.60	2.97	19.61	3.12	3.05
JS1	71.57	16.90 (20.60)	3.47	15.66 (19.61)	3.65	3.56
JS2	72.48	17.25 (20.60)	3.52	16.56 (19.61)	3.70	3.61
JS3	84.33	15.04 (20.60)	4.09	15.01 (19.61)	4.30	4.20

in control specimen. Estimation of yield displacement, ultimate displacement and displacement ductility is based on envelops of hysteretic loop for each specimen as shown in Fig. 10. Table 4 compares the displacement ductility factors of each specimen.

Ductility of specimens JS1 and JS2 are 3.56 and 3.61 respectively, or 16.7% and 18.4% greater than that of the control specimen. Effect of strengthening offered by skeleton reinforcements is not significant. Specimen JS3 using ferrocement jackets with one chamfer achieves the highest ductility at 4.20 (37.7% higher than that of the control specimen). This is mainly attributed to the increase in the ultimate deformation of beam, which is resulted from distribution of plastic hinge over a considerable distance at interface of strengthening and un-strengthening area in the beam. It suggests that one chamfer may have the advantage in enhancing ductility.

3.6 Joint shear stress

Joint shear stress in the joint region can be calculated as joint shear force V_{jh} divided by effective joint area A_j as seen in Eq. (1). Here, effective joint area is taken from joint region for control specimen and from combined joint and chamfer region for strengthened specimen. Determination of joint width is referred to ACI-ASCE 352R (2002). Horizontal joint shear force V_{jh} in an exterior beam-column joint can be computed by the following equation based on force equilibrium of a free body diagram in the joint as shown in Fig. 13.

$$v_{jh} = V_{jh} / A_j \tag{1}$$

$$V_{jh} = T - V_c \tag{2}$$

where T is the tensile force of beam reinforcements using Eq. (3) and V_c is the column shear force determined by Eq. (4).

$$T = V_b l_b^{'} / j_d \tag{3}$$

$$V_c = V_b (l_b + 0.5 h_c) / l_c \tag{4}$$

where V_b is the beam shear force which is the applied load. l_b and l_c are the lengths of beam and column respectively. $l_b^{'}$ is the length from loading point to column face for the control specimen (same as l_b) minus the depth of chamfers for strengthened specimens. j_d is the lever arm of beam section and is approximated to 0.85 h_b. h_b and h_c are the depths of beam and column respectively.

Calculated joint shear stresses using Eqs. (1)-(4) for all specimens are given in Table 3. Joint shear stress of the control specimen is $0.68\sqrt{f_c^{'}}$ MPa as compared with the lower boundary limit ($0.5\sqrt{f_c^{'}}$ MPa) for an exterior beam-column joint with volumetric ratio of transverse reinforcements less than 0.3% as specified in ASCE/SEI 41 (2007). As a result, joint shear failure is critical in the control specimen. In the absence of transverse reinforcements in the joint of the control specimen, shear stress within the joint could not satisfy ACI-ASCE 352R (2002). With strengthening by ferrocement jackets with chamfers, measured joint shear stresses are around $0.35\sqrt{f_c^{'}}$ MPa for strengthened specimens. Note that these joint shear stresses are the average values taken by horizontal joint areas (original joint and chamfer). The reduction in joint shear stress is contributed to the enlargement of effective joint area which consists of ferrocement-jacketed joint and

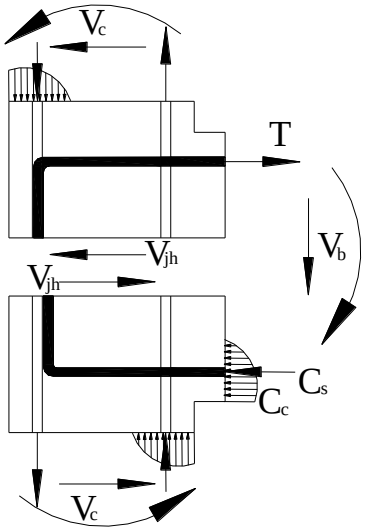

Fig. 13 Free-body diagram of exterior beam-column joints

chamfers. Measured shear stresses for all strengthened specimens are smaller than the specified value in ASCE/SEI 41 (2007). This is attributed to that beam flexural failure dominates failure mode of strengthened specimen. In other words, strengthened specimens do not reach their joint shear capacity at failure.

3.7 Joint shear distortion

Joint shear distortion is estimated from the readings of two diagonal LVDTs installed in the joint. Fig. 14 plots shear distortion against drift ratio for all specimens. Shear distortion of control specimen JC0 increases as drift ratio increases in both push and pull directions. This is due to the absence of transverse reinforcement to confine the joint. Shear distortions are similar for all strengthened specimens and maintain at small level as drift ratio increases. It demonstrates that relocation of plastic hinge away from the joint is beneficial to protect the joint. Moreover, redistribution of shear force within the joint decreases shear distortion. In general, all strengthening schemes using ferrocement jackets with chamfers are effective to reduce shear distortion of beam-column joints without transverse reinforcement.

3.8 Strains of beam reinforcements

Strains were measured at three critical locations at top reinforcements of the beams. Averaged values obtained from the readings at each location from two different reinforcements are given in Fig. 15, comparing the strains at peak strength against different drift ratios.

At the initial stage of loading (1.1% drift ratio), reinforcements in the joints and chamfers of all specimens remain elastic (with strains smaller than 2500 micron or yield strain of reinforcements). Strains of reinforcements in the control specimen increase quicker than that in strengthened specimens, especially within the joint. Reinforcements within the joint in the control specimen yield at a drift ratio of 1.4%. This is consistent with the observation as illustrated in Fig. 6(a). With progressive increase in drift ratio, difference in strains of reinforcements within the joint between

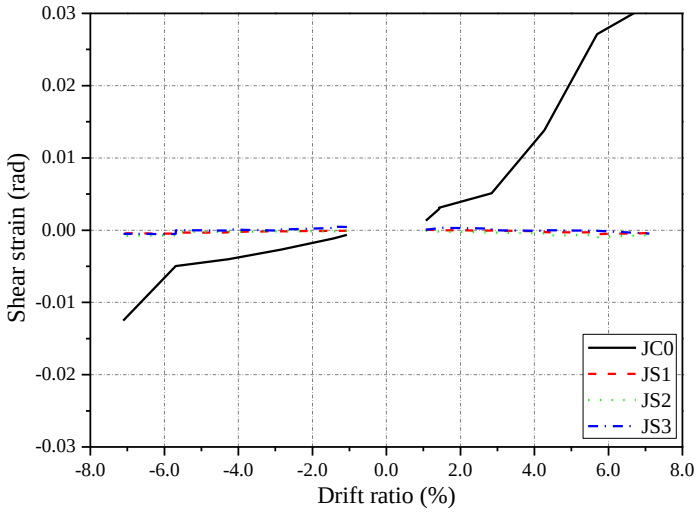

Fig. 14 Comparison of shear distortion against drift ratio for all specimens

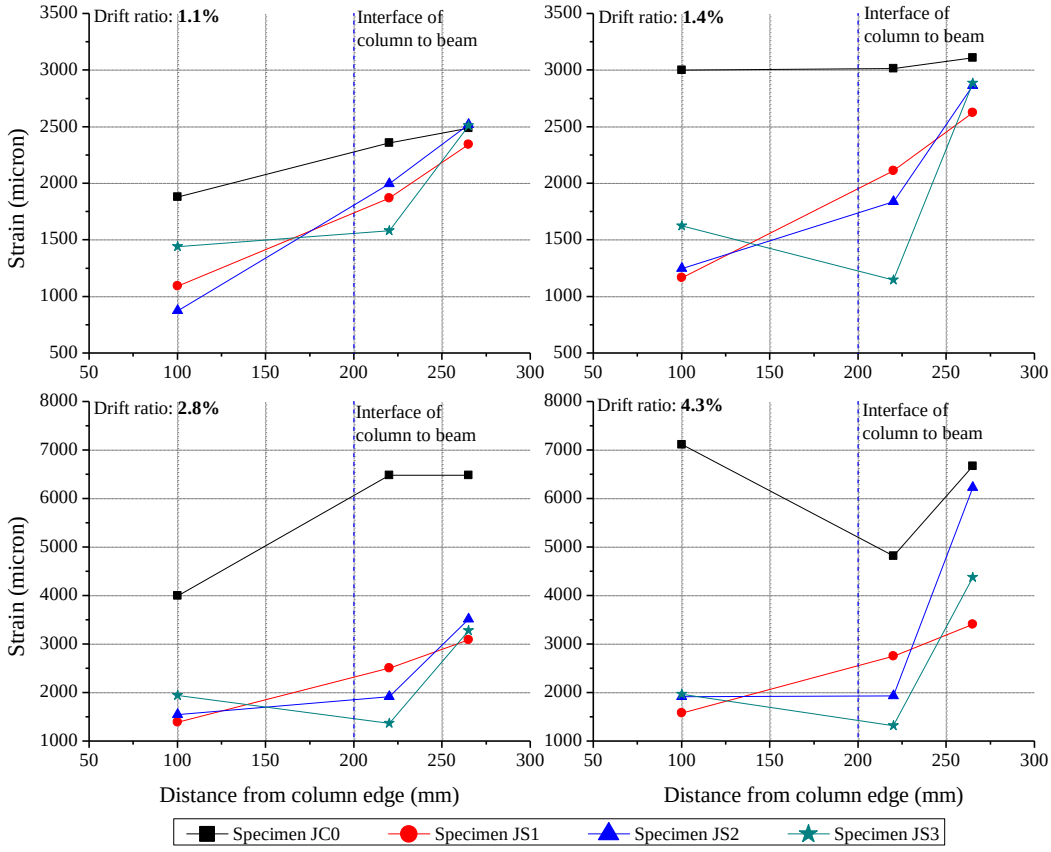

Fig. 15 Strain distribution of beam reinforcements at different drift ratios

the control specimen and strengthened specimens widens. Jacketed chamfers reduce strains of beam reinforcements within the joint and at beam-column interfaces. Reinforcements within the joints for the strengthened specimens remain elastic throughout the loading procedure. It implies the reduction of stress level within the joint, which is beneficial for preventing joint-shear failure. However, strains of reinforcements in the chamfers increase gradually due to strain penetration from plastic hinge zones and reach yielding value at 1.4% drift ratio. This is consistent with the occurrence of cracks in the chamfers at around 1.4% drift ratio. Subsequently, strains of reinforcements in the chamfers increase rapidly but do not penetrate into the joint. As the chamfers can limit the strain penetration into the joint, the proposed strengthening method is effective in reducing strains of reinforcements within the joint.

4. Design considerations

Test results has indicated that the proposed strengthening method is effective for protecting non-seismically designed beam-column joints through relocating plastic hinge away from the joint as well as reducing shear force transferred into the joint. To ensure plastic hinge relocating to a

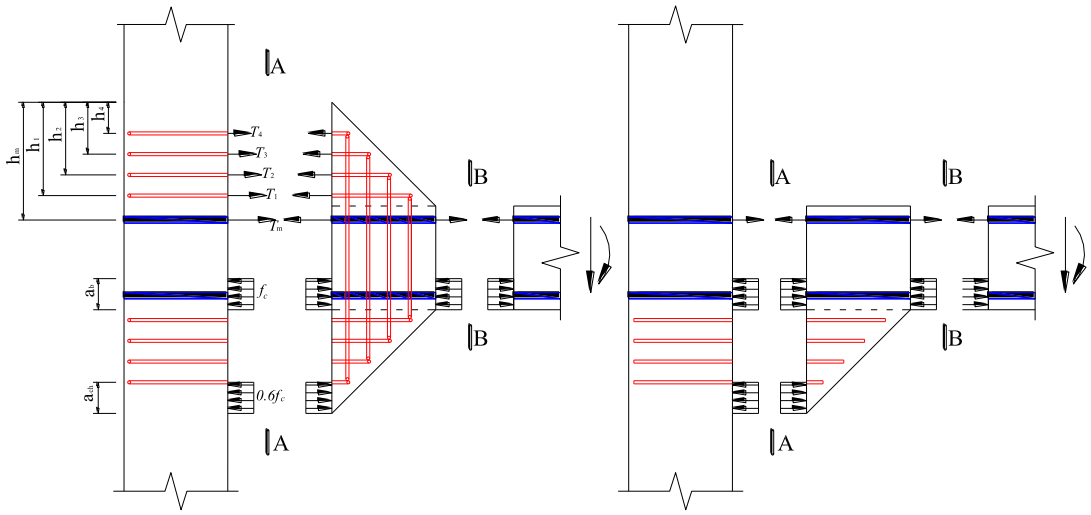

Fig. 16 Forces at two critical sections (A-A and B-B) of strengthened specimens

specific distance from the joint, flexural strengths at critical sections are checked to avoid yielding at beam-column interface.

Two critical sections are considered, namely sections A-A and B-B at column edge and at edge of chamfers respectively as shown in Fig. 16. For the strengthened specimens, additional moment capacity is provided between sections A-A and B-B by the ferrocement jackets with chamfers. This moves the plastic hinge away from the joint and suppresses possible joint failure. For proper development of plastic hinges in the un-strengthened area of the beams, flexural strength at section A-A must be ensured. Moment capacity at section A-A should be larger than moment demand extrapolated from plastic hinge adjacent to the chamfer. A simple method for calculating moment capacity at section A-A is presented using sectional analysis. It is noted that moment capacity at section A-A is estimated conservatively assuming reinforcement at beam-column interface remain elastic.

Fig. 17 shows strain distribution of skeleton reinforcements at different drift ratios in specimen JS1. Strains are obtained from strain gauges attached to skeleton reinforcements at the interface between chamfer and column (Fig. 17). Skeleton reinforcements remain elastic throughout the test with maximum strain of 580 micron at 4.3% drift ratio. Integrity of the chamfer with the joint is preserved. Skeleton reinforcements close to beam edge give the largest strain. Also, strain of skeleton reinforcements decreases gradually when moving away from beam edge. Based on the above, the following assumptions are used for estimating tensile force at beam-column interface for strengthened specimens.

(1) Strains in skeleton reinforcements are inversely proportional to the distance from the edge of beam;

(2) Maximum strain of skeleton reinforcements first occurs at the edge of beam;

(3) Effect of wire mesh in ferrocement is included using the same approximation in (1) and (2) above.

(4) Tensile stress contributed from concrete and mortar is neglected;

Thus, tensile force at beam-column interface for strengthened specimens can be computed using Eqs. (5) and (6).

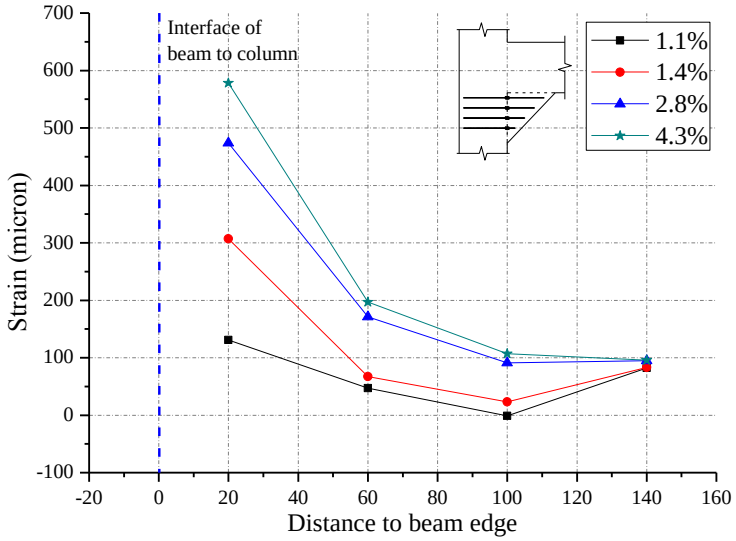

Fig. 17 Strain distribution of skeleton reinforcements at different drift ratios

$$T_t = T_m + \sum T_i = f_y A_s + \sum f_{ysi} A_i \tag{5}$$

$$f_{ysi} = \frac{h_i}{h_m} f_{ys} \tag{6}$$

where T_t is tensile force at beam-column interface; T_m and T_i are the tensile forces of longitudinal reinforcement and skeleton reinforcement (or equivalent wire mesh) respectively; f_y and f_{ys} are the yield strengths of longitudinal reinforcement and skeleton reinforcement respectively. f_{ysi} is the actual stress of skeleton reinforcement in ferrocement. A_i is the area of skeleton reinforcement (or equivalent wire mesh) at each location. h_m is the distance from longitudinal reinforcement to outside edge of chamfer. h_i is the distance of i^{th} skeleton reinforcement to outside edge of chamfer.

In the compression zone, two compressive stress blocks are formed based on strut-and-tie analysis as shown in Fig. 18. Depth of compression stress block at beam section is assumed to be the same as that at section B-B. Pimanmas and Chaimahawan (2010) recommended that width of concrete strut in the chamfer can be calculated using Eq. (7). Depth of compression zone in the chamfer is equal to $a_s/\cos\beta$.

$$a_s = 0.5(a_b \cos\beta + a_c \sin\beta) \tag{7}$$

$$a_c = (0.25 + 0.85n)h_c \tag{8}$$

where a_b and a_c are the depths of compression stress blocks at beam and column respectively; β is the angle of concrete strut in the chamfer; n is the axial load ratio; h_c is the depth of column section. a_b at section B-B is calculated under ultimate state considering 1.25 factor for strength of reinforcement. a_c is computed using Eq. (8) in Paulay and Priestley (1992). According to Pimanmas and Chaimahawan (2010), stress in concrete strut in the beam is larger than that in the chamfer. Concrete stress of compression block at chamfer is found to be about 60% of that at beam

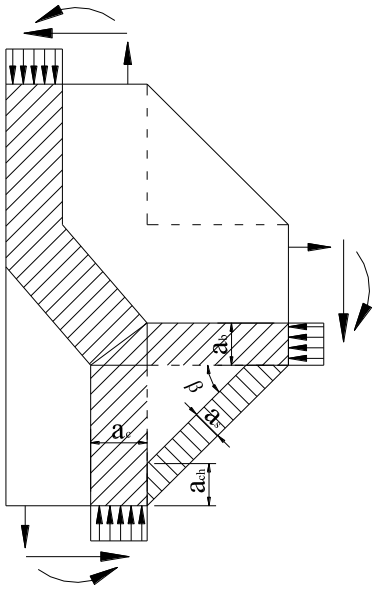

Fig. 18 Concrete struts formed in the joint region

section based on strut-and-tie analysis. However, it should be noted that concrete stress should be limited to 0.51 $f_c^{'}$ which is effective strength of concrete strut without crack control reinforcement in ACI 318 (2011). This limitation is set for preventing failure of concrete strut before developing moment capacity at section A-A. Based on force equilibrium at section A-A, concrete stresses at both compression stress blocks can be derived.

Based on the above, moment capacities at section A-A for specimens JS1 and JS2 are 70.3 kNm and 50.8 kNm respectively. Positive (tension at bottom) and negative moment capacities for specimen JS3 are 34.5 kNm and 48.5 kNm respectively. It is noted that positive moment capacity in specimen JS3 is calculated considering yielding of all equivalent wire mesh due to the reduction in depth of the section. With the contribution of skeleton reinforcement, moment capacity at section A-A of specimen JS1 is significantly higher than moment demand. Calculated moment capacities of other strengthened specimens are slightly greater than the applied moment at section A-A at ultimate limit state for the joint. Thus, plastic hinge can be formed in the un-strengthened area of beam next to the chamfer. Generally, the proposed estimation for beam-column interface in strengthened specimens gives reasonable results, though it may be conservative as section A-A did not yield in the test.

5. Conclusions

This paper presents an experimental study on strengthening of non-seismically designed beam-column joints by plastic hinge relocation. Ferrocement jackets with chamfers are utilized to achieve plastic hinge relocation as well as shear force input reduction. Based on the experimental results and observations, the following conclusions can be drawn.

• Beam-column joint without transverse reinforcement fails in joint-shear mode followed by axial failure of the column with buckling of longitudinal reinforcements.

• The proposed strengthening method using ferrocement jackets with chamfers is effective for relocating plastic hinge from the joint to the un-strengthened area of beam. As a result, seismic performance in terms of peak horizontal load, energy dissipation, stiffness and ductility of beam-column joints is enhanced.

• Averaged joint shear stress is reduced from $0.68\sqrt{f_c'}$ MPa in the control specimen to around $0.35\sqrt{f_c'}$ MPa in the strengthened specimens. It verifies relocation of plastic hinge using ferrocement jacketed chamfers can decrease shear force input to the joint. This can be contributed to force redistribution within the joint and increase in effective joint area using chamfers with reliable integration with the joint.

• Shear distortion of joint core and strains of beam reinforcements within the joint are reduced after strengthening. This is beneficial for protecting non-seismically designed beam-column joint from damage.

• Generally, contribution of skeleton reinforcements to ferrocement jackets is limited. It slightly increases energy dissipation, initial stiffness and ductility, but has significant improvement on crack control.

• Comparing specimens strengthened by ferrocement jackets with two chamfers and one chamfer, the latter exhibits slight reduction in peak strength and energy dissipation, but an increase in ductility. Considering the benefit in space, it is suggested to strengthen beam-column joints using ferrocement jackets with one chamfer. For beam-column joints with more reinforcement in upper side of the beam, i.e., design for negative moment, one chamfer is preferred to be installed at the soffit of the beams.

Acknowledgements

The authors are grateful to the financial support from The Hong Kong Polytechnic University and the Research Grants Council of Hong Kong (RGC No: PolyU 5206/08E). The authors would like to thank the technical assistance provided by Structural Engineering Research Laboratory and Concrete Technology Laboratory of The Hong Kong Polytechnic University.

References

Abdel-Fattah, B. and Wight, J.K. (1987), "Study of moving beam plastic hinging zones for earthquake-resistant design of R/C buildings", *ACI Struct. J.*, **84**(1), 31-39.

ACI-ASCE 352R-02 (2002), *Recommendations for Design of Beam-column Connections in Monolithic Reinforced Concrete Structures*, American Concrete Institute, Farmington Hills, MI.

ACI 549R (1997), *State-of-the-Art Report on Ferrocement*, ACI Committee 549, Detroit, MI.

ACI 318-11 (2011), *Building Code Requirements for Structural Concrete (ACI 318-11) and Commentary*, American Concrete Institute, Farmington Hills, MI.

Alcocer, S.M. and Jirsa, J.O. (1993), "Strength of reinforced-concrete frame connections rehabilitated by jacketing", *ACI Struct. J.*, **90**(3), 249-261.

Alsayed, S.H., Al-Salloum, Y.A., Almusallam, T.H. and Siddiqui, N.A. (2010), "Seismic response of FRP-upgraded exterior RC beam-column joints", *J. Compos. Constr.*, **14**(2), 195-208.

Antonopoulos, C.P. and Triantafillou, T.C. (2003), "Experimental investigation of FRP-strengthened RC beam-column joints", *J. Compos. Constr.*, **7**(1), 39-49.

ASCE/SEI 41 (2007), *Seismic Rehabilitation of Existing Buildings*, American Society of Civil Engineers,

Reston, VA.
Bousselham, A. (2010), "State of research on seismic retrofit of RC beam-column joints with externally bonded FRP", *J. Compos. Constr.*, **14**(1), 49-61.
Chaimahawan, P. and Pimanmas, A. (2009), "Seismic retrofit of substandard beam-column joint by planar joint expansion", *Mater. Struct.*, **42**(4), 443-459.
Chutarat, N. and Aboutaha, R.S. (2003), "Cyclic response of exterior reinforced concrete beam-column joints reinforced with headed bars - experimental investigation", *ACI Struct. J.*, **100**(2), 259-264.
Copconcrete (1987), *Code of Practice for the Structural Use of Concrete-1987*, Buildings and Lands Department, Hong Kong.
Engindeniz, M., Kahn, L.F. and Zureick, A.H. (2005), "Repair and strengthening of reinforced concrete beam-column joints: state of the art", *ACI Struct. J.*, **102**(2), 187-197.
Genesio, G., Eligehausen, R. and Pampanin, S. (2011), "Application of post-installed anchors for seismic retrofit of RC beam-column joints: design method", *Proceeding of the 9th Pacific Conference on Earthquake Engineering Building an Earthquake-Resilient Society*, Auckland, New Zealand.
Ghobarah, A., Aziz, T.S. and Biddah, A. (1997), "Rehabilitation of reinforced concrete frame connections using corrugated steel jacketing", *ACI Struct. J.*, **94**(3), 283-294.
Ghobarah, A. and Said, A. (2002), "Shear strengthening of beam-column joints", *Eng. Struct.*, **24**(7), 881-888.
Hakuto, S., Park, R. and Tanaka, H. (2000), "Seismic load tests on interior and exterior beam-column joints with substandard reinforcing details", *ACI Struct. J.*, **97**(1), 11-25.
Ilki, A., Bedirhanoglu, I. and Kumbasar, N. (2011), "Behavior of FRP-retrofitted joints built with plain bars and low-strength concrete", *J. Compos. Constr.*, **15**(3), 312-326.
Kam, W.Y., Pampanin, S. and Elwood, K. (2011), "Seismic performance of reinforced concrete buildings in the 22 February Christchurch (Lyttelton) earthquake", *Bull. NZ. Soc. Earthq. Eng.*, **44**(4), 239-278.
Karayannis, C.G., Chalioris, C.E. and Sideris, K.K. (1998), "Effectiveness of RC beam-column connection repair using epoxy resin injections", *J. Earthq. Eng.*, **2**(2), 217-240.
Karayannis, C.G. and Sirkelis, G.M. (2008), "Strengthening and rehabilitation of RC beam-column joints using carbon-FRP jacketing and epoxy resin injection", *Earthq. Eng. Struct. Dyn.*, **37**(5), 769-790.
Karayannis, C.G., Chalioris, C.E. and Sirkelis, G.M. (2008), "Local retrofit of exterior RC beam-column joints using thin RC jackets - an experimental study", *Earthq. Eng. Struct. Dyn.*, **37**(5), 727-746.
Lam, S.S.E., Xu, Y.L., Chau, K.T., Wong, Y.L. and Ko, J.M. (2002), "Progress in earthquake resistant design of buildings in Hong Kong", *Proceeding of Structural Engineering World Congress*, Yokohama, Japan.
Li, B. and Chua, H.Y.G. (2009), "Seismic performance of strengthened reinforced concrete beam-column joints using FRP composites", *J. Struct. Eng.*, ASCE, **135**(10), 1177-1190.
Li, B. and Qian, K. (2011), "Seismic behavior of reinforced concrete interior beam-wide column joints repaired using FRP", *J. Compos. Constr.*, **15**(3), 327-338.
Li, B., Lam, E.S.S., Wu, B. and Wang, Y.Y. (2013), "Experimental investigation on reinforced concrete interior beam-column joints rehabilitated by ferrocement jackets", *Eng. Struct.*, **56**, 897-909.
Mahini, S.S. and Ronagh, H.R. (2011), "Web-bonded FRPs for relocation of plastic hinges away from the column face in exterior RC joints", *Compos. Struct.*, **93**(10), 2460-2472.
Naaman, A.E. (2000), *Ferrocement and Laminated Cementitious Composites*, Techno Press 3000.
Pampanin, S., Christopoulos, C. and Chen, T.H. (2006), "Development and validation of a metallic haunch seismic retrofit solution for existing under-designed RC frame buildings", *Earthq. Eng. Struct. Dyn.*, **35**(14), 1739-1766.
Pantelides, C.P., Okahashi, Y. and Reaveley, L.D. (2008), "Seismic rehabilitation of reinforced concrete frame interior beam-column joints with FRP composites", *J. Compos. Constr.*, **12**(4), 435-445.
Park, R. (1989), "Evaluation of ductility of structures and structural assemblages from laboratory testing", *Bull. NZ. Soc. Earthq. Eng.*, **22**(3), 155-166.
Paulay, T. and Priestley, M.J.N. (1992), *Seismic Design of Reinforced Concrete and Masonry Buildings*, A Wiley Interscience publication, John Wiley & Sons, INC.

Pimanmas, A. and Chaimahawan, P. (2010), "Shear strength of beam-column joint with enlarged joint area", *Eng. Struct.*, **32**(9), 2529-2545.

Prota, A., Nanni, A., Manfredi, G. and Cosenza, E. (2004), "Selective upgrade of underdesigned reinforced beam-column joints using carbon fiber-reinforced concrete", *ACI Struct. J.*, **101**(5), 699-707.

Sasmal, S., Ramanjaneyulu, K., Novak, B., Srinivas, V., Kumar, K. S., Korkowski, C., Roehm, C., Lakshmanan, N. and Iyer, N.R. (2011), "Seismic retrofitting of nonductile beam-column sub-assemblage using FRP wrapping and steel plate jacketing", *Constr. Build. Mater.*, **25**(1), 175-182.

Sezen, H., Whittaker, A.S., Elwood, K.J. and Mosalam, K.M. (2003), "Performance of reinforced concrete buildings during the August 17, 1999 Kocaeli, Turkey earthquake, and seismic design and construction practise in Turkey", *Eng. Struct.*, **25**(1), 103-114.

Sezen, H. (2012), "Repair and strengthening of reinforced concrete beam-column joints with fiber-reinforced polymer composites", *J. Compos. Constr.*, **16**(5), 499-506.

Su, R.K.L. and Wong, S.M. (2007), "A survey on axial load ratios of structural walls in medium-rise residential buildings in Hong Kong", *HKIE Tran.*, **14**(3), 40-46.

Yi, W.H., You, Y.C. and Lee, L.H. (1996), "Moving and spreading beam plastic hinging zones for the ductile behavior of high-strength beam plastic hinging zones for the ductile behavior of high-strength reinforced concrete beam", *Proceeding of 11th World Conference on Earthquake Engineering*, Paper No. 384.

CC